Japan Bilingual Publishing Co.

New Environmentally-Friendly Materials
https://ojs.bilpub.com/index.php/nefm

ARTICLE

Electrochemical Energy Storage Studies on Sustainably Synthesized Co3O4 Nanoparticles for Supercapacitor Electrodes

Helen Osora [1], ***T. Jebakumar Immanuel Edison*** [2], ***David Kolkoma*** [1], ***Gabriel Anduwan*** [1], ***Mathew Waimbo*** [1], ***Senthilkumar Velusamy*** [1*]

[1] *School of Applied Physics, Papua New Guinea Univers·ity of Technology, Lae 411, Papua New Guinea*
[2] *Department of Chemistry, Sethu Institute of Technology, Kariapatti 626115, India*

ABSTRACT

In this study, a facile hydrothermal technique was used, and the commercially important cobalt oxide nanoparticles were synthesised for pseudocapacitor electrodes in supercapacitor applications. The prepared particles were subjected to different characterization techniques to determine their phase structure, topography, and elemental composition by XRD, FE-SEM, TEM, and EDAX. The XRD pattern confirmed the formation of pure cubic spinel Co_3O_4 phase with well-defined diffraction peaks and without any impurity phases, indicating high crystallinity of the synthesized nanoparticles. In addition, Raman spectroscopy exhibited prominent vibrational modes at around 469, 514, and 684 cm^{-1}, corresponding to the F_2g and A_1g modes of the spinel Co_3O_4 structure, further confirming the successful formation of phase-pure cobalt oxide with strong crystalline quality. Further, the particles electrochemical properties were investigated in an alkaline electrolyte at 3 M. The electrochemical studies confirmed that during galvanostatic charge and discharge studies, the built electrode displays a maximal specific capacitance value of 450 Fg^{-1} at 6 Ag^{-1}. In addition, the cyclic stability experiments confirmed that the prepared electrode exhibits a retaining ability of 87% even after cycles at 10 Ag^{-1}. Further, the constructed symmetrical structure achieved a highest power density of 1312

*CORRESPONDING AUTHOR:
Senthilkumar Velusamy, School of Applied Physics, Papua New Guinea University of Technology, Lae 411, Papua New Guinea; Email: velusamy.senthilkumar@pnguot.ac.pg

ARTICLE INFO
Received: 24 August 2025 | Revised: 20 September 2025 | Accepted: 27 September 2025 | Published Online: 4 October 2025
DOI: https://doi.org/10.55121/nefm.v4i2.689

CITATION
Osora, H., Edison, T.J.I., Kolkoma, D., et al., 2025. Electrochemical Energy Storage Studies on Sustainably Synthesized Co_3O_4 Nanoparticles for Supercapacitor Electrodes. New Environmentally-Friendly Materials. 4(2): 1–13. DOI: https://doi.org/10.55121/nefm.v4i2.689

W kg^{-1} with an energy density of 19 Wh kg^{-1}, measured at a current density of 10 Ag^{-1}. These results demonstrate that hydrothermally synthesized Co_3O_4 nanoparticles are promising, low-cost, environmentally benign electrode materials for high-power supercapacitor applications such as power buffering in renewable-energy systems and short-duration backup for portable electronics.

Keywords: Hydrothermal; Supercapacitor; Cyclic Voltammetry; Symmetrical Device

1. Introduction

An issue of paramount importance for both established and emerging nations is the world's energy consumption rising annually, highlighting the critical need for renewable energy sources that are both clean and environmentally friendly [1–3]. Consequently, researchers are concentrating on a potential alternative solution to this problem by enhancing energy conversion and storage systems [4–7]. In the energy storage device category, supercapacitor exceeds secondary batteries in several ways, including eco-friendliness, charging speed, cycle life, and energy density [8,9]. In recent years, glucose-derived carbon has attracted attention in energy storage because of its renewable source, tunable porosity, and good conductivity. It has been combined with transition metal oxides to improve capacitance, though challenges remain with stability, rate capability, and cycle life [10–15]. Research on active materials for pseudocapacitor electrode applications, metal oxides and their hydroxides, has gained significant importance in recent years due to their enormous capacitance and quick redox kinetics [16]. Several transition metal oxides, including ZnO, NiO, MnO_2, and RuO_2 [17–20], are widely used as pseudocapacitor electrodes due to their multiple oxidation states, different shapes, and structures that improve electrochemical performance through reversible redox reactions. Among those materials, researchers are particularly interested in Co_3O_4 nanoparticles due to their unique characteristics and applications [21]. Co_3O_4 nanoparticles are used in sensors, catalysis, batteries, capacitors, field emission materials, and magneto-resistive devices [22–24]. Particularly, cobalt oxides and their forms are identified as an emerging material for use in supercapacitors. For its cost-effectiveness, high theoretical C_s (3560 Fg^{-1}), strong redox activity, and environmental friendliness [25]. The cobalt oxide's spinel structure is formed by the position of oxide ions in a cubic close packing (CCP) array. Inside this structure, the Co^{2+} and Co^{3+} ions occur in the tetrahedral 8a and octahedral 16d sites, respectively. Notably, Co_3O_4 is an easily reducible oxide material because of its low barriers for oxygen vacancies and weak Co-O bond strength. This makes it a very good choice for use as an electrode in supercapacitors [26]. Supercapacitors need to be viewed alongside other storage technologies such as lithium-ion batteries and fuel cells. Although supercapacitors have lower energy density, they provide faster charging and longer cycle life. Progress in batteries includes scalable microwave-assisted production of $Ti_3C_2TxMXene$ for Li-ion and Na-ion systems [27]. For supercapacitors, NiFe-LDH/PANI composites made via microwave-assisted methods have also shown strong performance [28]. Together, these studies highlight both competition and complementarity between different energy storage systems. Furthermore, it is well known that the performance of supercapacitors is significantly impacted by the crystallographic structure and crystallinity, shape, surface area, combination of chemical elements, and framework stability of nanostructured materials. Due to these merits, extensive work has been focused on synthesising Co_3O_4 with controlled size, morphology, and crystal structure [29,30]. The hydrothermal technique is frequently used to synthesise nanostructured materials, which have the advantages of easy control of size, shape, crystal structure, and low reaction temperature. Also, nanomaterials with high vapor pressures can be generated by the hydrothermal process with low material loss [31].

In this work, the Co_3O_4 nanoparticles are synthesised using a straightforward hydrothermal technique for their implementation as an electrode in supercapacitors. The crystalline phase and morphological properties of synthesised Co_3O_4 nanoparticles were analysed by XRD, FE-SEM, and TEM measurements. The chemical stability, oxidation process, and capacitive behavior of the prepared Co_3O_4-based electrode were investigated through an electrochemical workstation. Finally, a symmetrical device is fabricated and tested for its energy density and power density.

2. Experimental Methodology

2.1. Preparation of Nano-Sized Cobalt Oxide (Co3O4) Particles

All the compounds have been used without any additional purification. The synthesis comprised stirring 0.5 g of cobalt (II) acetate tetrahydrate (Co $(CH_3CO_2)_2 \cdot 4\ H_2O$) with 75 mL of ethanol in a magnetic stirring device for an hour to get a clear solution. In another beaker, 0.05 g of sodium carbonate ($Na_2CO_3 \cdot 10H_2O$) was dissolved in 20 mL of ethanol. Further, both solutions were combined and placed into a hydrothermal unit. The temperature of the reaction was held steady at 170 °C for a duration of 16 hours. Once the material reached the surrounding temperature, it underwent many rounds of centrifugation using ethanol and deionized water. Finally, to characterize, followed by electrode preparation, the obtained compound was annealed for one hour at 500 °C. **Figure 1** illustrates an exploded diagram of the complete hydrothermal processing steps for the synthesis of Co_3O_4 nanoparticles.

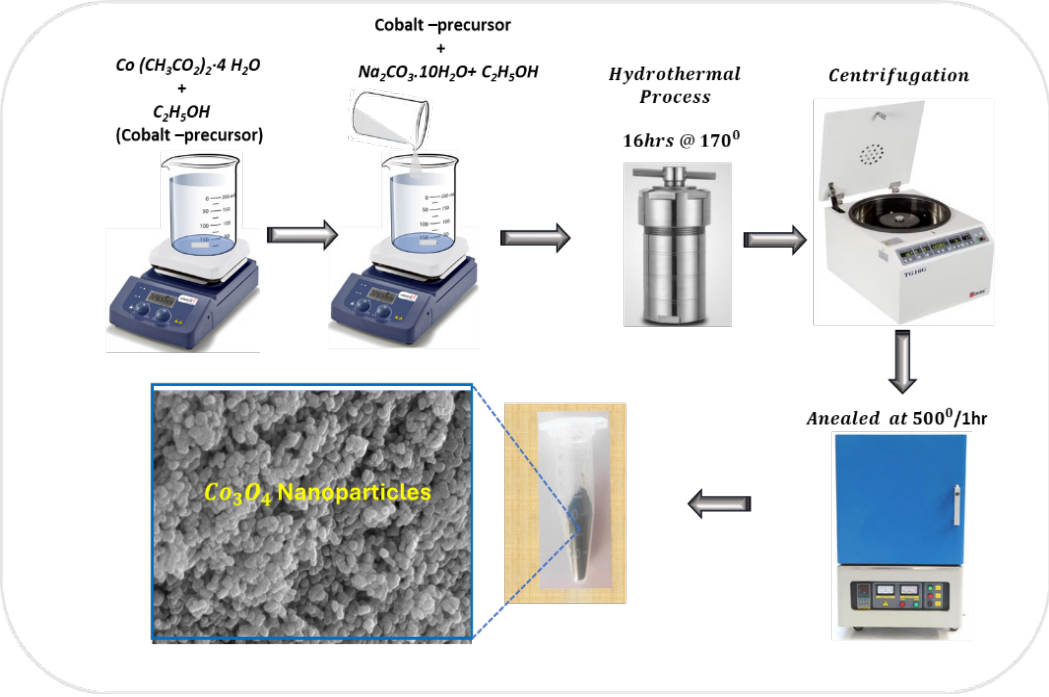

Figure 1. A schematic outline representing the synthesis procedure for Co_3O_4 nanoparticles.

2.2. Material Characterizations

The XRD measurements were conducted by Malvern PANalytical instruments to determine the crystalline form of the samples that were prepared. The composition, particle dimensions, and surface morphology were examined, incorporating a field emission scanning electron microscope (FESEM, ZEISS SmartSEM, Germany) and a high-resolution transmission electron microscope (HR-TEM, JEOL JEM 2010, performed at 200 kV). Raman spectra were acquired by using a confocal Raman microscope (WITec alpha 300 RA, Ulm, Germany) that featured a 532 nm excitation wavelength green laser.

2.3. Electrochemical Characterization

Electrochemical efficacy was assessed by employing a GAMRY electrochemical workstation (Model: Interface 1010E) with a 3M KOH aqueous electrolyte at ambient temperature. The working electrode was constructed by preparing a paste that included 80% produced active material, 10% porous carbon, and 10% PVDF in NMP solvent. This mixture was uniformly applied onto pre-cleaned nickel foam using a pressing process. To ensure adequate adhesion and get rid of residual solvent, the coated electrodes had been dried at 80 °C for 15 h. A three-electrode setup was employed, incorporating a silver reference electrode

and a platinum foil to be the counter electrode. The electrochemical characteristics of the prepared electrodes were carefully investigated through cyclic voltammetry (CV), galvanostatic charge-discharge (GCD) tests, and impedance spectroscopy (EIS).

3. Results and Discussion

3.1. Structural and Morphological Studies

The XRD diffraction patterns of the synthesised cobalt oxide are presented in Figure 2.

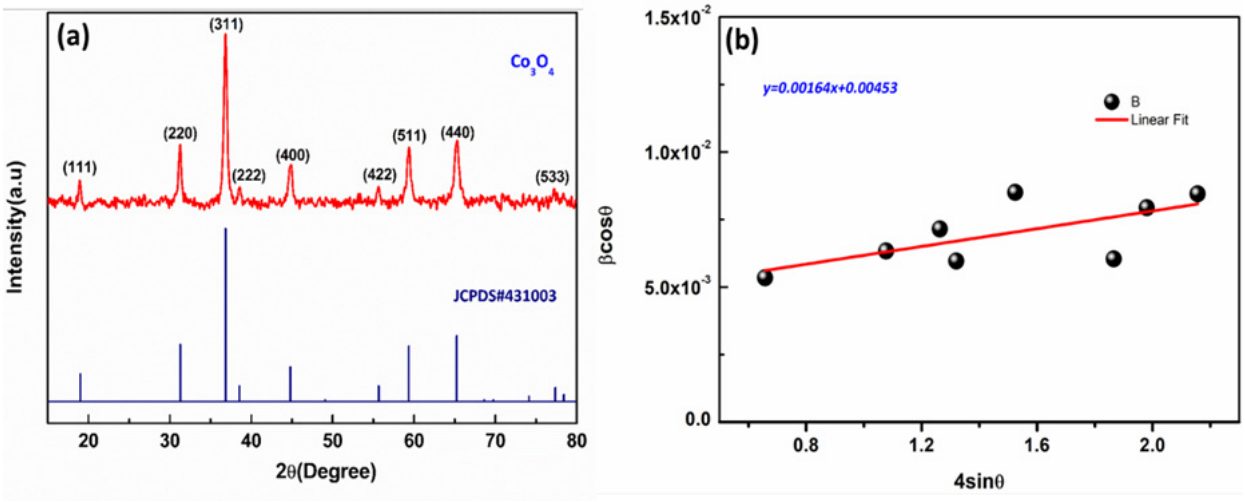

Figure 2. XRD profile of CO3O4 nanoparticles (**a**) and (**b**) Williamson-Hall plot.

Noticeable diffraction peaks at 18.98, 31.17, 36.88, 38.50, 44.74, 55.45, 59.22, 65.07, 74.11, and 77.38, which correspond to reflections from the planes (1 1 1), (2 2 0), (3 1 1), (2 2 2), (4 0 0), (4 2 2), (5 1 1), (4 4 0), and (5 3 3). The obtained peaks are well aligned with the face-centred cubic crystallographic structure of the Fd3m space group (JCPDS:431003). The XRD spectrum depicts the absence of other impurity-related peak profiles, thus indicating higher purity of Co_3O_4. Further, high-intensity peaks indicate that the synthesised powders are crystalline in nature. The Deby-Sherrer equation was applied to determine the average crystallite size, as shown below [32,33]:

$$D=\frac{k\lambda}{\beta_{(hkl)}\cos\theta_{(hkl)}}$$

Here, k, λ, β, and θ represent the Scherrer constant (0.89), X-ray source wavelength, FWHM of the diffraction peak, and the Bragg reflection angle, correspondingly. The estimated average crystallite size was determined to be 23 nm. Additionally, the crystallite size was further analysed using the Williamson-Hall method, applying the following equation [34].

$$\beta\cos\theta=\frac{k\lambda}{D}+4\varepsilon\sin\theta$$

In Figure 2, the y-intercept of the linear fit relates to the crystallite size, whereas the slope of the fitted line reflects the lattice strain within the material. The synthesised $C_{o3}O4$ nanoparticles had a lattice strain of and an extracted particle size of 32 nm. The Sherrer formula yields a lower calculated crystallite size for C_o3O4 than the W-H plot methods. In general, intrinsic micro-strain in nanocrystals is caused by stacking defects, point defects, triple junctions, and grain boundaries [35]. Hence, the broadening of X-ray diffraction peaks is additionally influenced by lattice strain and defects. The higher crystallite size value derived from the W-H plot estimates peak broadening by factoring in the enlargement of the diffraction peak width as a function of 2θ, which incorporates lattice strain and defects, whereas the Sherrer equation considers only peak broadening [36].

Further, FE-SEM was implemented to examine the surface profile and microstructural characteristics associated with the Co_3O_4 nano-sized particles, as presented in

Figure 3. Noticeably, the particles are well-crystallised nanocrystals with weakly agglomerated assemblies. The agglomeration is mainly caused by the coulombic force between the particles due to the Van der Waals force. The size of the particles was determined and indexed utilizing ImageJ software, as in **Figure 3**.

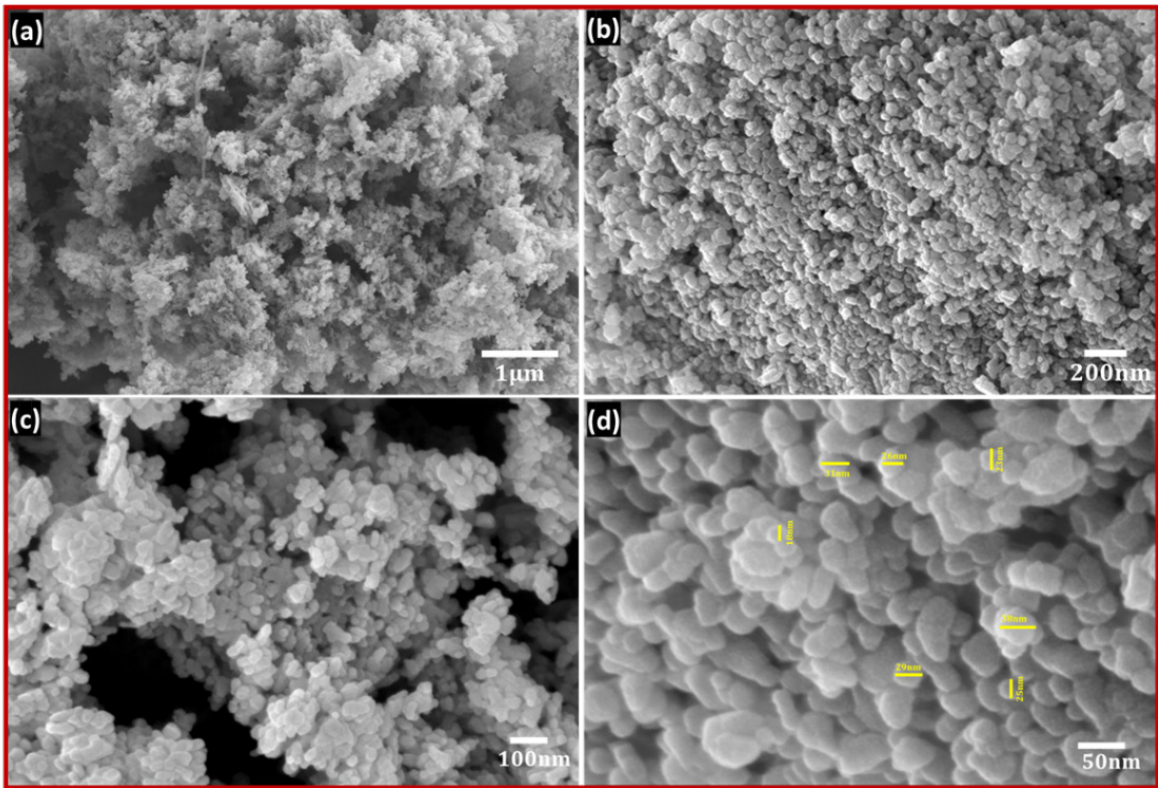

Figure 3. FE-SEM pictures of Co3O4 nanoparticles with low to high magnifications.

The measured average particle size is closely matched with the XRD results. Additionally, a mapping examination was conducted to investigate the chemical composition of cobalt (Co) and oxygen (O) components in the scanning electron microscope. The mapping images of the selected area, the mixed cobalt and oxygen, cobalt (Co), and oxygen (O), are shown in **Figure 4**. The mapping survey images demonstrate that Co and O are uniformly distributed, and as a result, the elemental chemical composition ratio is almost in near proximity. EDAX analyses were conducted to inspect the purity and stoichiometry. As displayed in **Figure 4**, it is clearly shown that Co and O only appeared in the EDAX spectrum. The other two peaks, around 0.28 and 2.15 keV, are caused by the conducting carbon tape and sputtered Au. The atomic weight % of cobalt (Co) and oxygen (O) were determined to be 60.02% and 39.98%, respectively. These values closely align with the expected ratio of Co_3O_4. No additional elemental traces can be found, confirming the high purity of the Co_3O_4 nanoparticles.

Figure 5 displays the transmission electron microscopy image of Co3O4 nanoparticles with different magnifications. TEM analysis provides information on the size, shape, and state of aggregation of the Co3O4 nanoparticles. The TEM picture in Figure 4 reveals that the Co3O4nanoparticles are in an irregular shape, and the measured particle size lies in the range of 17–31 nm, which agrees with the XRD and FE-SEM measurements. The measured interplanar distance value of 0.24 nm corresponds to the reflection plane of (311) for cubic Co3O4 (refer Figure 5). It is also clearly evidenced from the SAED pattern of Figure 5 that the prepared Co3O4 is crystalline in nature. According to the SAD pattern, the diameter of each diffraction ring is proportional to $\sqrt{h^2+k^2+l^2}$, where (hkl) denotes the Miller indices of the respective planes.The measured diffraction fringe pattern corresponds to the (2 2 0), (3 1 1), (2 2 2), (4 0 0), (4 2 2), (5 1 1), and (4 4 0) planes, which are in line with the peak profiles re-

ported in the XRD results.

Raman analysis is an effective technique to determine the sample's purity as well as its oxygen vacancies, the degree of crystallinity, stacking faults, and size effects of the nanoparticles. The spinal structure of Co_3O_4 crystallises in the cubic Fd3m space group. For the Fd3m symmetry, the space group theory predicts the following active modes. From the aforesaid vibrations, and are Raman active modes. Among the vibrations originated from modes, four are vibrations of infrared active Raman modes, whereas one is a vibration of the acoustic mode. The other existing vibrations (, , and) are the inactive modes of Co_3O_4 [37]. The room temperature Raman spectrum of the Co_3O_4 is presented in **Figure 6**.

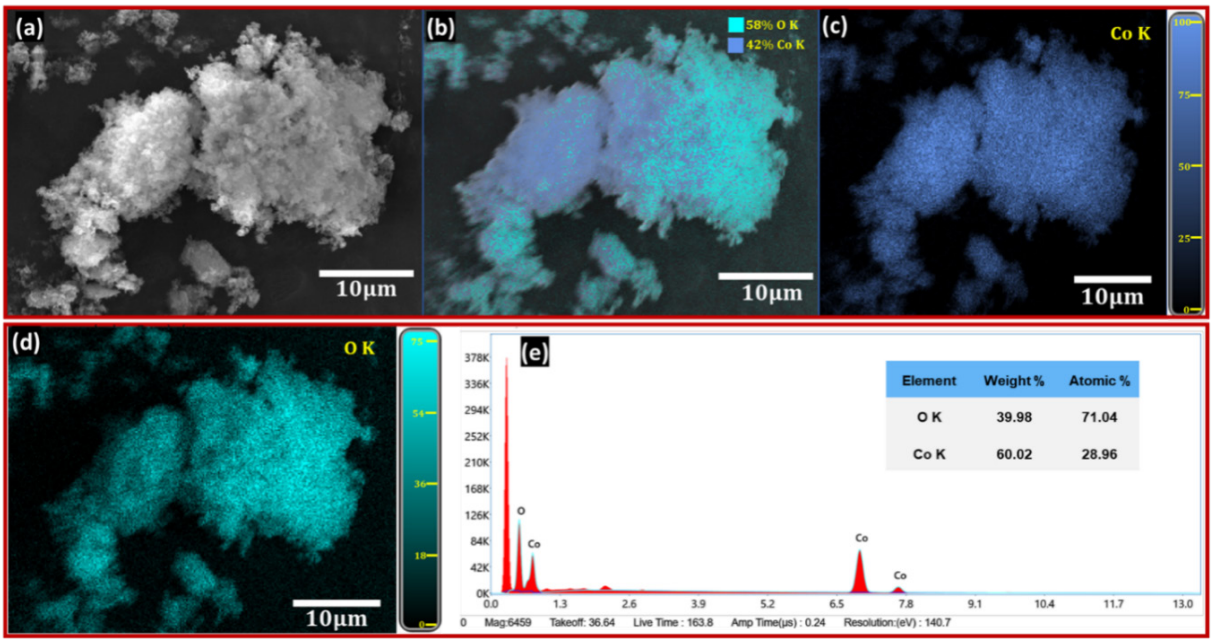

Figure 4. The selected area for the elemental mapping of Co3O4 nanoparticles (**a**), the overlapping of cobalt and oxygen (**b**), elemental mapping for cobalt (**c**), oxygen (**d**), and the EDX spectrum (**e**).

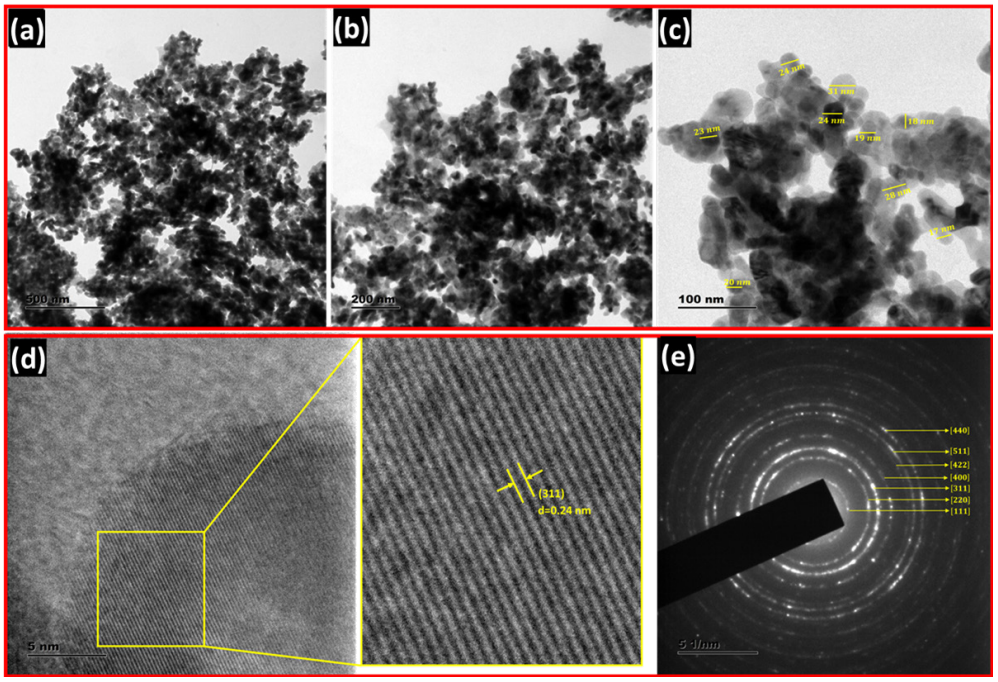

Figure 5. TEM picture of cobalt oxide at different magnifications (**a**–**c**), high-resolution TEM picture (**d**), and SAED pattern (**e**).

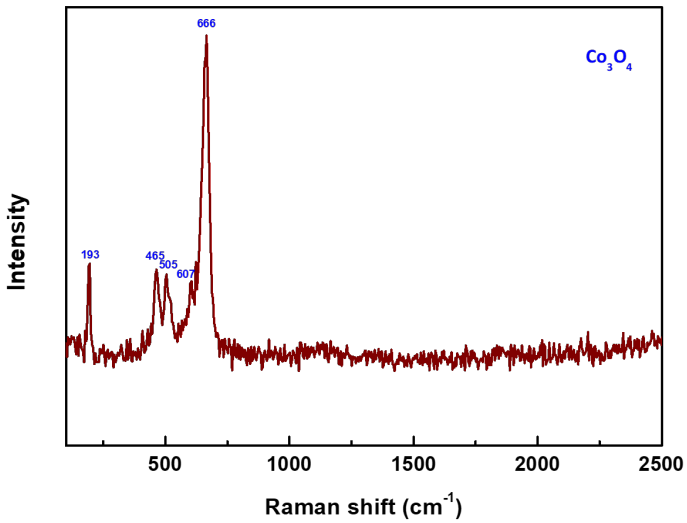

Figure 6. Raman spectra of Co3O4 nanoparticles.

The strongest peak at 666 cm^{-1} showed the typical characteristics of the octahedral sites of A_{1g} mode, whereas the peaks at 193, 505, and 607 cm^{-1} were classified as F_{2g} mode. The vibration at 465 cm^{-1} was related to the E_g modes of Raman active vibration. The E_g and F_{2g} modes were linked to the corresponding vibrations of tetrahedral and octahedral oxygen motions [38]. The minor shift seen at the peak can also be explained by size-dependent effects or by stresses and strains developed by the surface. The positions of the peaks are consistent with those previously recorded for crystalline Co_3O_4 [39]. The low intensity with the broadened nature of the peaks establishes the formation of nanocrystalline Co_3O_4. The results obtained from the Raman spectrum agreed well with the XRD results.

3.2. Electrochemical Analysis

The cyclic voltametric test for the Co_3O_4 nanoparticle electrode was conducted in a 3M KOH aqueous electrolyte with diverse scan speeds, as depicted in **Figure 7**. The applied working potential window was fixed between −0.25 and 0.3 V. It is clear from the CV curve that there are two significant oxidation peaks (A_1 and A_2) and the related two reduction peaks (C_1 and C_2) in the range of 0.07–0.24 V and −0.05–0.12 V, respectively (refer **to Figure 7**). The oxidation and reduction peaks that were seen are caused by reversible redox transitions from Co^{+2} to Co^{+3} and Co^{+3} to Co^{+4}. On the basis of the Co_3O_4 electrode CV profiles in an alkaline medium, the two redox couples that were observed may be explained by the following redox processes [40,41].

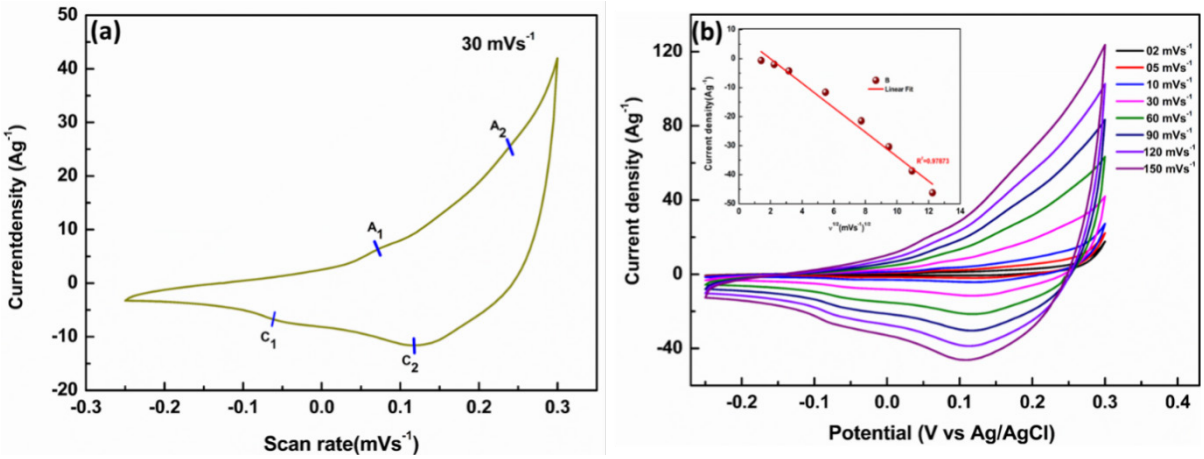

Figure 7. (**a**) Cyclic voltammetry profile of Co3O4 electrode at 30mVs-1 and (**b**) different scan speeds (inset: reduction peak current density vs scan speed).

$$Co_3O_4 + H_2O + OH^- \rightleftharpoons 3CoOOH + e^-$$

$$CoOOH + OH^- \rightleftharpoons CoO_2 + H_2O + e^-$$

The redox pairs of A_1 and $C_1$from the CV profile indicate the electron transfer process between Co^{+2} and Co^{+3}. During the reaction, there is a reversible intercalation of ions into Co_3O_4, which is then reduced to CoOOH. As a result, the electrode's charge storage capacity is enhanced via pseudocapacitance. The A_2 and C_2 redox peaks indicate the transformation of Co^{+3} from Co^{+4} due to the adsorption of ions on the near surface, which thus produces CoO_2 during the reduction process. The process is irreversible and non-faradaic, although it still contributes to capacitance. The deviation of the CV curve from a rectangular shape suggests that the charge-storing mechanism is attributed to the pseudocapacitive process, which arises from reversible redox reactions [42,43]. The distortions of CV curves upon positive and negative scans reflect irreversible redox features that are controlled by polarization effects, along with the ohmic resistance experienced through the process of Faradaic process [44]. Additionally, the inset in **Figure 7** reveals an almost linear dependence between the oxidation peak current density and the scanning rate. The confirmed existence of surface redox processes supports the characteristics of the pseudocapacitive electrode behaviour of Co_3O_4.

Enhanced cycle reliability and higher-rate discharge capabilities are necessary for the material to be successfully utilised for supercapacitive electrode applications. The charge/discharge evaluation was done for the Co_3O_4 electrode with numerous current densities over a potential range of −0.25 to 0.25 V, as presented in **Figure 8**. The nonlinear structure of the discharge curve confirms that Co_3O_4 exhibits pseudocapacitive behaviour due to adsorption/desorption along with the redox processes triggered within the electrode and electrolyte interface [37,45]. The Co_3O_4 electrode's specific capacitance (C_s) was determined using the GCD curves from the relationship as follows [46,47]:

$$C_s = \frac{\text{Discharge current(I)} \times \text{Discharge time}\backslash(\Delta t\backslash)}{\text{Active material mass(m)} \times \text{Voltagerange}\backslash(\Delta V\backslash)}$$

The specific capacitance (Cs) of the Co_3O_4 electrode at different current densities is displayed in **Figure 8**.

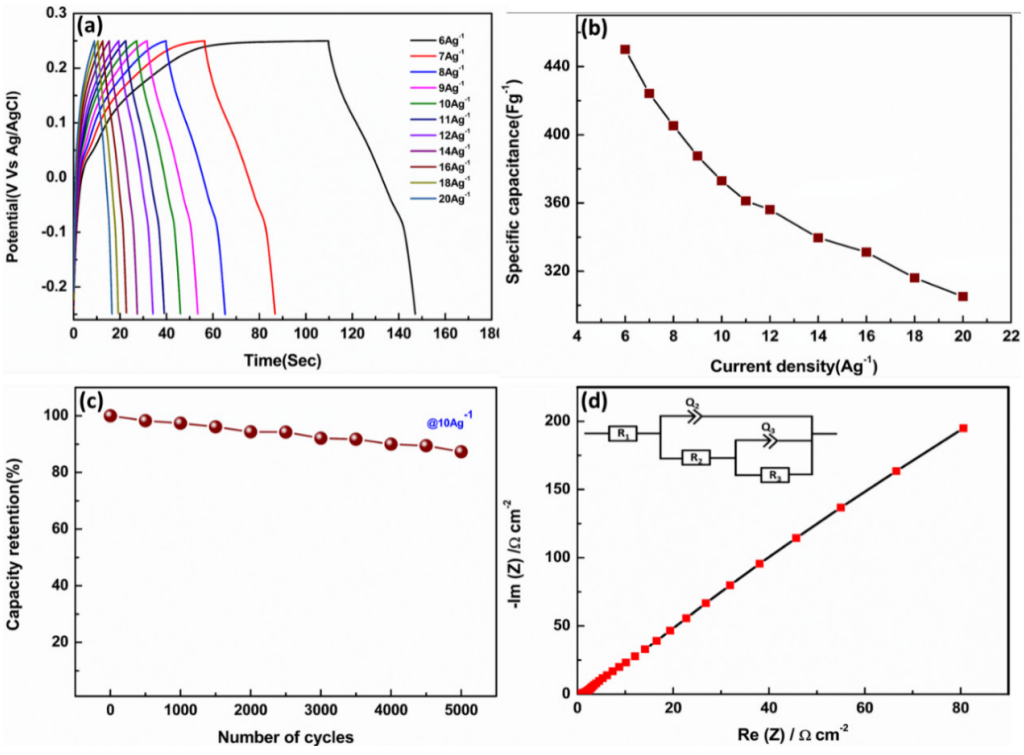

Figure 8. (**a**) Galvanostatic charge-discharge (GCD) analysis of the Co_3O_4 electrode at different current densities; (**b**) Specific capacitance (C_s) variation as a function of current density; (**c**) Cycling stability and capacity retention over multiple charging-discharging cycles; and (**d**) Impedance profile of the Co_3O_4.

The electrode achieves a maximum specific capacitance (Cs) of 450 F g^{-1} at a current density of 6 A g^{-1}. Even when the current density increases to 20 A g^{-1}, the capacitance remains at 305 F g^{-1}, demonstrating that the electrode has efficient charge storage capability. Assessing the electrode's cycling stability is essential to evaluate its structural integrity and electrochemical durability in supercapacitor applications. To examine the durability of the material, the Co_3O_4 electrode carried out continuous charge-discharge cycles under an applied current density of 10 A g^{-1}. As demonstrated in **Figure 8**, the electrode preserved 89% of its original capacitance, confirming its robustness and sustained electrochemical behavior. These findings underscore the material's potential for reliable energy storage in supercapacitors.

The Nyquist graph analysis for the Co_3O_4 electrode in 3M KOH is seen in **Figure 8**. It is observed from the figure that there is a minute semicircle in the higher frequency range and a slanting line in the lower frequency range, which represents the presence of double-layer capacitance along with the supercapacitance of Co_3O_4. The obtained Nyquist plot is exactly compatible with the proposed equivalent circuit presented in **Figure 8**. The total resistance and capacitance of the Co_3O_4 electrode in KOH are about 10 Ω/cm^2 and 3.124 μF/cm^2, which are obtained from the fitted results, respectively. The low resistance and good conductivity of the Co_3O_4 electrode strongly suggest it can be applied as a supercapacitor [48,49].

The performance and efficiency of electrochemical supercapacitors are significantly defined by the criteria of energy and power density. To verify these properties, a symmetrical device was fabricated using a Swagelok cell. Each electrode contained 0.32 mg of active material, giving a total loading of 0.64 mg. A Whatman filter paper was used as the separator in a 3 M KOH electrolyte. **Figure 9** depicts the CV profile, galvanostatic charging/discharging profiles, and calculated capacitance values of a Co_3O_4// Co_3O_4 symmetrical device. **Figure 9** presents the CV profiles at various scan speeds for the device operating within a potential range of −0.3 to 0.8 V.

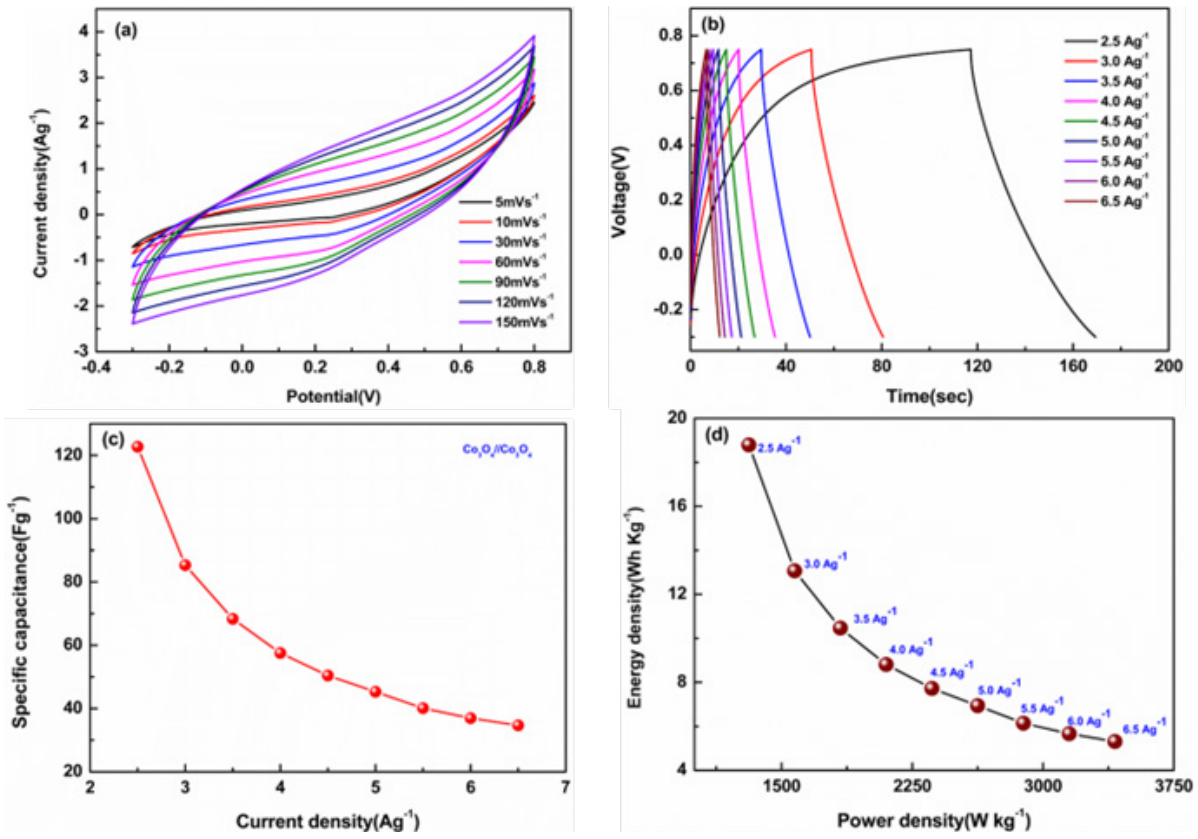

Figure 9. Electrochemical efficacy results of Co_3O_4//Co_3O_4 symmetric device: (**a**) CV profiles at various sweep rates; (**b**) GCD profiles at various current densities; (**c**) measured specific capacitance for different current densities; (**d**) energy density versus power density plot.

The structure of the CV profile remains the same without any redox peaks while increasing the scan speeds, indicating that the built-in device has excellent reversibility, rate capability, and a moderate operating cell voltage [50]. **Figure 9** depicts the galvanostatic charge/discharge curves for the Co_3O_4//Co_3O_4 symmetrical device at various applied current densities ranging from 2.5 to 6.5 Ag^{-1}. With an increase in current density, the discharge time decreases, and the charge-storing efficacy of the symmetric supercapacitor device decreases because electrolytic ions cannot effectively reach all of the active sites. Furthermore, IR drops at the initial portion of the discharge curve are due to the internal resistance of the symmetrical device. To evaluate the energy and power densities of the symmetrical device, the measured capacitance value and discharging time were used and derived by using the following relationship [51,52]:

$$\text{Energy density (ED)} = \frac{C_s \times \Delta V^2}{2 \times 3.6}$$

$$\text{Power density (PD)} = \frac{ED \times 3600}{\Delta t}$$

Where Cs, and ΔV are the specific capacitance (C_s) calculated from the two-electrode system, discharging time, and operating potential window, respectively. **Figure 9** depicts the energy density vs. power density curve for the Co_3O_4//Co_3O_4 symmetrical device. The device displays a maximum energy density value of 19 Wh kg^{-1} and a power density of 1312 W kg^{-1} at a current density of 2.5 Ag^{-1}, which are consistent with the previously published reports [53]. Based on the previously discussed research findings, Co_3O_4 has demonstrated significant potential as an intriguing electrode material for pseudocapacitor uses in supercapacitors. Its outstanding electrochemical characteristics, including rich specific capacitance and redox activity, as well as stability, allow it to be an attractive option for enhancing energy storage performance in advanced supercapacitor systems.

4. Conclusions

To summarize, a simple, cost-effective hydrothermal process was employed to synthesize Co_3O_4 nanoparticles for supercapacitor electrode applications. The XRD profile confirmed that the synthesized Co_3O_4 nanoparticle had a face-centered cubic crystal structure. In addition, Raman analysis also supports the XRD results. The GCD measurements showed the Co_3O_4 electrode delivered a maximum capacitance of 450 Fg^{-1} at a current density of 6 Ag^{-1} in a 3M KOH aqueous electrolyte. The Co_3O_4 electrode preserved 87% of its initial capacitance following successive charge-discharge cycles at a current density of 10 A g^{-1}. Furthermore, the assembled symmetric supercapacitor proved a peak energy density of 19 Wh kg^{-1} and a power output of 1312 W kg^{-1} when evaluated at a current density of 2.5 A g^{-1}.

Author Contributions

Conceptualization, H.O. and D.K.; methodology, H.O.; software, H.O.; validation, T.J.I.E., G.A. and M.W.; formal analysis, H.O.; investigation, H.O.; resources, H.O.; data curation, H.O.; writing—original draft preparation, H.O. and D.K.; writing—review and editing, S.V.; visualization, H.O.; supervision, S.V.; project administration, H.O.; funding acquisition, D.K. All authors have read and agreed to the published version of the manuscript.

Funding

Not applicable.

Institutional Review Board Statement

Not applicable.

Informed Consent Statement

Not applicable.

Data Availability Statement

Not applicable.

Conflicts of Interest

The authors declare that there are no conflict of interest.

References

[1] Hu, X., Wei, L., Chen, R., et al., 2020. Reviews and Prospectives of Co_3O_4-Based Nanomaterials for Supercapacitor Application. Chemistry Select. 5(17), 5268–5288. DOI: https://doi.org/10.1002/slct.201904485

[2] Zhang, J., Gu, M., Chen, X., 2023. Supercapacitors for Renewable Energy Applications: A Review. Micro Nano Engineering. 100229. DOI: https://doi.org/10.1016/j.mne.2023.100229

[3] Muzaffar, A., Ahamed, M.B., Deshmukh, K., et al., 2019. A Review on Recent Advances in Hybrid Supercapacitors: Design, Fabrication and Applications. Renewable and Sustainable Energy Reviews. 101, 123–145. DOI: https://doi.org/10.1016/j.rser.2018.10.026

[4] Gogotsi, Y., Simon, P., 2011. True Performance Metrics in Electrochemical Energy Storage. Science. 334(6058), 917–918. DOI: https://doi.org/10.1126/science.1213003

[5] Wei, T.Y., Chen, C.H., Chien, H.C., et al., 2010. A Cost-Effective Supercapacitor Material of Ultrahigh Specific Capacitances: Spinel Nickel Cobaltite Aerogels from an Epoxide-Driven Sol–Gel Process. Advanced Materials. 22(3), 347–351. DOI: https://doi.org/10.1002/ADMA.200902175

[6] Martha, S.K., Pappu, S., Sarada, B.V., et al., 2022. Concept of Thermodynamic Studies in Electrochemical Storage and Conversion Systems. Encyclopedia of Energy Storage. 1, 264–274. DOI: https://doi.org/10.1016/B978-0-12-819723-3.00135-9

[7] Najib, S., Erdem, E., 2019. Current Progress Achieved in Novel Materials for Supercapacitor Electrodes: Mini Review. Nanoscale Advances. 1(8), 2817–2827. DOI: https://doi.org/10.1039/C9NA00345B

[8] Gür, T.M., 2018. Review of Electrical Energy Storage Technologies, Materials and Systems: Challenges and Prospects for Large-Scale Grid Storage. Energy & Environmental Science. 11(10), 2696–2767. DOI: https://doi.org/10.1039/C8EE01419A

[9] Osora, H., Kolkoma, D., Anduwan, G., et al., 2024. Hydrothermally Grown SnO_2 and SnO_2/rGO Nanocomposite and Its Physio-Electrochemical Studies for Pseudocapacitor Electrode Applications. Journal of Cluster Science. 35(3), 891–901. DOI: https://doi.org/10.1007/s10876-023-02517-5

[10] Lokhande, P.E., Kadam, V., Jagtap, C., 2024. Comparative Performance of Aqueous and Ionic Liquid-Based Gel Electrolytes in $Co(OH)_2$/rGO-Based Supercapacitor. Energy Technology. 12, 2400995. DOI: https://doi.org/10.1002/ente.202400995

[11] Lokhande, P.E., Chavan, U.S., 2020. Cyclic Voltammetry Behavior Modeling of Fabricated Nanostructured $Ni(OH)_2$ Electrode Using Artificial Neural Network for Supercapacitor Application. Proceedings of the Institution of Mechanical Engineers, Part C: Journal of Mechanical Engineering Science. 234(13), 2563–2568. DOI: https://doi.org/10.1177/0954406220907615

[12] Lokhande, P.E., Chavan, U.S., 2019. Inorganic Electrolytes in Supercapacitor. Materials Research Foundations. 61, 11–30. DOI: https://doi.org/10.21741/9781644900499-2

[13] Lokhande, P.E., Chavan, U.S., Deokar, S., et al., 2019. Surfactant-Free Chemically Deposited Wheat Spike-Like Nanostructure on Cu Foam for Supercapacitor Applications. Materials Today: Proceedings. 18, 979–985. DOI: https://doi.org/10.1016/j.matpr.2019.06.537

[14] Mohite, D.D., Chavan, S.S., Dubal, S., et al., 2024. Electrochemical Evaluation of ZnO and PAN-Based Carbon Nanofibers Composite for High-Performance Supercapacitor Application. Ionics. 30(12), 8469–8480. DOI: https://doi.org/10.1007/s11581-024-05869-8

[15] Lokhande, P.E., Kadam, V., Jagtap, C., et al., 2025. Fast Synthesis of Co3O4-MXene Nanocomposites via Microwave Assistance for Energy Storage Applications. Diamond and Related Materials. 154, 112191. DOI: https://doi.org/10.1016/j.diamond.2025.112191

[16] Wang, Y., Lei, Y., Li, J., et al., 2014. Synthesis of 3D-Nanonet Hollow Structured Co3O4 for High Capacity Supercapacitor. ACS Applied Materials & Interfaces. 6(9), 6739–6747. DOI: https://doi.org/10.1021/am500464n

[17] Samuel, E., Joshi, B., Kim, M.W., et al., 2019. Hierarchical Zeolitic Imidazolate Framework-Derived Manganese-Doped Zinc Oxide Decorated Carbon Nanofiber Electrodes for High-Performance Flexible Supercapacitors. Chemical Engineering Journal. 371, 657–665. DOI: https://doi.org/10.1016/j.cej.2019.04.065

[18] Senthilkumar, V., Kadumudi, F.B., Ho, N.T., et al., 2016. NiO Nanoarrays of a Few Atoms Thickness on 3D Nickel Network for Enhanced Pseudocapacitive Electrode Applications. Journal of Power Sources. 303, 363–371. DOI: https://doi.org/10.1016/j.jpowsour.2015.11.034

[19] Zhu, G., He, Z., Chen, J., et al., 2014. Highly Conductive Three-Dimensional MnO2–Carbon Nanotube–Graphene–Ni Hybrid Foam as a Binder-Free Supercapacitor Electrode. Nanoscale. 6(2), 1079–1085. DOI:

https://doi.org/10.1039/C3NR04495E

[20] Wu, Z.S., Wang, D.W., Ren, W., et al., 2010. Anchoring Hydrous RuO2 on Graphene Sheets for High-Performance Electrochemical Capacitors. Advanced Functional Materials. 20(20), 3595–3602. DOI: https://doi.org/10.1002/adfm.201001054

[21] Farahmandjou, M., 2016. Fabrication and Characterization of Nanoporous Co Oxide (Co_3O_4) Prepared by Simple Sol–Gel Synthesis. Physical Chemistry Research. 4(2), 153–160. DOI: https://doi.org/10.22036/pcr.2016.12909

[22] Li, W.Y., Xu, L.N., Chen, J., 2005. Co_3O_4 Nanomaterials in Lithium-Ion Batteries and Gas Sensors. Advanced Functional Materials. 15(5), 851–857. DOI: https://doi.org/10.1002/adfm.200400429

[23] Ping, Y., Zhang, H., Meng, S., 2025. Reduced Graphene Oxide/Porous Cobalt Oxides With Oxygen Vacancies as Electrode Materials for High-Performance Supercapacitor. Diamond and Related Materials. 158, 112694. DOI: https://doi.org/10.1016/j.diamond.2025.112694

[24] Casas-Cabanas, M., Binotto, G., Larcher, D., et al., 2009. Defect Chemistry and Catalytic Activity of Nanosized Co_3O_4. Chemistry of Materials. 21(9), 1939–1947. DOI: https://doi.org/10.1021/cm900328g

[25] Rabani, I., Yoo, H.S., Kim, H.S., et al., 2021. Highly Dispersive Co_3O_4 Nanoparticles Incorporated into a Cellulose Nanofiber for a High-Performance Flexible Supercapacitor. Nanoscale. 13(1), 355–370. DOI: https://doi.org/10.1039/D0NR06982E

[26] Zhang, Y., Tang, Y., Liu, X., et al., 2012. Three-Dimensional CdS-Titanate Composite Nanomaterials for Enhanced Visible-Light-Driven Hydrogen Evolution. Small. 9(7), 996–1002. DOI: https://doi.org/10.1002/smll.201202156

[27] Sharma, R.K., Sharma, S., Dutta, S., et al., 2015. Fe_3O_4 (Iron Oxide)-Supported Nanocatalysts: Synthesis, Characterization and Applications in Coupling Reactions. Green Chemistry. 18(11), 3207–3230. DOI: https://doi.org/10.1039/C6GC00864J

[28] Lokhande, P.E., Khasim, S., Hamdalla, T.A., et al., 2025. Electrochemical Evaluation of NiFe-LDH/PANI Based Composite Electrode Synthesized via Microwave Assisted Method for Supercapacitor Application. Inorganic Chemistry Communications. 179, 114802. DOI: https://doi.org/10.1016/j.inoche.2025.114802

[29] Deng, M.J., Huang, F.L., Sun, I.W., et al., 2009. An Entirely Electrochemical Preparation of a Nano-Structured Cobalt Oxide Electrode with Superior Redox Activity. Nanotechnology. 20(17), 175602. DOI: https://doi.org/10.1088/0957-4484/20/17/175602

[30] Yan, N., Hu, L., Li, Y., et al., 2012. Co_3O_4 Nanocages for High-Performance Anode Material in Lithium-Ion Batteries. Journal of Physical Chemistry C. 116(12), 7227–7235. DOI: https://doi.org/10.1021/jp2126009

[31] Agarwal, K., Mondal, S., Rai, H., 2023. Quantum Dots: An Overview of Synthesis, Properties, and Applications. Materials Research Express. 10(6), 062001. DOI: https://doi.org/10.1088/2053-1591/acda17

[32] Senthilkumar, V., Vickraman, P., Jayachandran, M., et al., 2010. Structural and Optical Properties of Indium Tin Oxide (ITO) Thin Films with Different Compositions Prepared by Electron Beam Evaporation. Vacuum. 84, 864–869. DOI: https://doi.org/10.1016/j.vacuum.2009.11.017

[33] Edison, T.N.J.I., Baral, E.R., Lee, Y.R., et al., 2016. Biogenic Synthesis of Silver Nanoparticles Using Cnidium officinale Extract and Their Catalytic Reduction of 4-Nitroaniline. Journal of Cluster Science. 27, 285–298. DOI: https://doi.org/10.1007/s10876-015-0929-z

[34] Prabhu, Y.T., Rao, K.V., Kumar, V.S.S., et al., 2014. X-Ray Analysis by Williamson-Hall and Size-Strain Plot Methods of ZnO Nanoparticles with Fuel Variation. World Journal of Nano Science and Engineering. 4(1), 21–28. DOI: https://doi.org/10.4236/wjnse.2014.41004

[35] Kushwaha, P., Chauhan, P., 2021. Microstructural Evaluation of Iron Oxide Nanoparticles at Different Calcination Temperature by Scherrer, Williamson-Hall, Size-Strain Plot and Halder-Wagner Methods. Phase Transitions. 94(10), 731–753. DOI: https://doi.org/10.1080/01411594.2021.1969396

[36] Das, R., Sarkar, S., 2015. Determination of Intrinsic Strain in Poly (Vinylpyrrolidone)-Capped Silver Nano-Hexapod Using X-Ray Diffraction Technique. Current Science. 109(4), 775–778. Available from: https://www.jstor.org/stable/24905739 (cited 16 August 2025).

[37] Kumarage, G.W.C., Zappa, D., Mihalcea, C.G., et al., 2023. Revolutionizing n-type Co3O4 Nanowire for Hydrogen Gas Sensing. Advanced Energy and Sustainability Research. 4, 2300067. DOI: https://doi.org/10.1002/aesr.202300067

[38] Sivachidambaram, M., Vijaya, J.J., Kaviyarasu, K., et al., 2017. A Novel Synthesis Protocol for Co_3O_4 Nanocatalysts and Their Catalytic Applications. RSC Advances. 7, 38861–38870. DOI: https://doi.org/10.1039/C7RA06996K

[39] Rivas-Murias, B., Salgueiriño, V., 2017. Thermody-

namic CoO–Co_3O_4 Crossover Using Raman Spectroscopy in Magnetic Octahedron-Shaped Nanocrystals. Journal of Raman Spectroscopy. 48(6), 837–841. DOI: https://doi.org/10.1002/jrs.5129

[40] Samal, R., Dash, B., Sarangi, C.K., et al., 2017. Influence of Synthesis Temperature on the Growth and Surface Morphology of Co_3O_4 Nanocubes for Supercapacitor Applications. Nanomaterials. 7(11), 356. DOI: https://doi.org/10.3390/nano7110356

[41] Premlatha, S., Chandrasekaran, M., Bapu, G.N.K.R., 2017. Preparation of Cobalt-RuO_2 Nanocomposite Modified Electrode for Highly Sensitive and Selective Determination of Hydroxylamine. Sensors and Actuators B: Chemical. 252, 375–384. DOI: https://doi.org/10.1016/j.snb.2017.06.013

[42] Conway, B.E., 2013. Electrochemical Supercapacitors: Scientific Fundamentals and Technological Applications. Springer Science and Business Media: Berlin/Heidelberg, Germany. pp. 1–685.

[43] Meher, S.K., Justin, P., Ranga Rao, G., 2011. Microwave-Mediated Synthesis for Improved Morphology and Pseudocapacitance Performance of Nickel Oxide. ACS Applied Materials & Interfaces. 3(6), 2063–2073. DOI: https://doi.org/10.1021/am200294k

[44] Pell, W.G., Conway, B.E., 2001. Voltammetry at a de Levie Brush Electrode as a Model for Electrochemical Supercapacitor Behaviour. Journal of Electroanalytical Chemistry. 500(1–2), 121–133. DOI: https://doi.org/10.1016/S0022-0728(00)00423-X

[45] Wang, X., Li, M., Chang, Z., et al., 2015. Co_3O_4@MWCNT Nanocable as Cathode with Superior Electrochemical Performance for Supercapacitors. ACS Applied Materials & Interfaces. 7(4), 2280–2285. DOI: https://doi.org/10.1021/am5062272

[46] Yan, S-X., Yan, X., Tian, X., et al., 2024. Elevation of the Electrochemical Stability Performance of Co3O4/g-C3N4 for an Asymmetric Supercapacitor. 38(17), 17076–17086. DOI: https://doi.org/10.1021/acs.energyfuels.4c03229

[47] Senthilkumar, V., Kim, Y.S., Chandrasekaran, S., et al., 2015. Comparative Supercapacitance Performance of CuO Nanostructures for Energy Storage Device Applications. RSC Advances. 5(26), 20545–20553. DOI: https://doi.org/10.1039/C5RA00035A

[48] Edison, T.N.J.I., Atchudan, R., Karthik, N., et al., 2017. Ultrasonic Synthesis, Characterization and Energy Applications of Ni–B Alloy Nanorods. Journal of the Taiwan Institute of Chemical Engineers. 80, 901–907. DOI: https://doi.org/10.1016/j.jtice.2017.07.034

[49] Edison, T.N.J.I., Atchudan, R., Lee, Y.R., 2018. Binder-Free Electro-Synthesis of Highly Ordered Nickel Oxide Nanoparticles and Its Electrochemical Performance. Electrochimica Acta. 283, 1609–1617. DOI: https://doi.org/10.1016/j.electacta.2018.07.101

[50] Chodankar, N.R., Dubal, D.P., Ji, S.H. et al., 2018. Superfast Electrodeposition of Newly Developed $RuCo_2O_4$ Nanobelts over Low-Cost Stainless Steel Mesh for High-Performance Aqueous Supercapacitor. Advanced Materials Interfaces. 5(15), 1800283. DOI: https://doi.org/10.1002/admi.201800283

[51] Liu, X., Lu, Y., Xiao, G., et al., 2023. MnO_2 Loaded Flower-Like Carbon Microspheres Derived from Polyimides for High-Performance Supercapacitors. Electrochimica Acta. 454, 142417. DOI: https://doi.org/10.1016/j.electacta.2023.142417

[52] Ji, S.-H., Chodankar, N.R., Kim, D.-H., 2019. Aqueous Asymmetric Supercapacitor Based on RuO_2–WO_3 Electrodes. Electrochimica Acta. 325, 134879. DOI: https://doi.org/10.1016/j.electacta.2019.134879

[53] Howli, P., Das, S., Sarkar, S., et al., 2017. Co_3O_4 Nanowires on Flexible Carbon Fabric as a Binder-Free Electrode for All Solid-State Symmetric Supercapacitor. ACS Omega. 2(8), 4216–4226. DOI: https://doi.org/10.1021/acsomega.7b00702